How to make a spiral bacterium

Charles W Wolgemuth[1]**, Yuki F Inclan**[2]**, Julie Quan**[3]**, Sulav Mukherjee**[4]**, George Oster**[5] **and M A R Koehl**[3]

[1] Department of Cell Biology, University of Connecticut Health Center, Farmington,
CT 06030-3505, USA
[2] Biophysics Graduate Group, University of California, Berkeley, CA 94720-3202, USA
[3] Department of Integrative Biology, University of California, Berkeley, CA 94720-3140, USA
[4] Department of Biomedical Engineering, University of Connecticut, Storrs, CT 06269-2247, USA
[5] Departments of Molecular & Cellular Biology and ESPM, University of California, Berkeley,
CA 94720-3112, USA

Abstract
The motility of some kinds of bacteria depends on their spiral form, as does the virulence of
certain pathogenic species. We propose a novel mechanism for the development of spiral shape
in bacteria and the supercoiling of chains ('filaments') of many cells. Recently discovered
actin-like proteins lying just under the cell wall form fibers that play a role in maintaining cell
shape. Some species have a single actin-like fiber helically wrapped around the cell, while
others have two fibers wrapped in the same direction. Here, we show that if these fibers
elongate more slowly than growth lengthens the cell, the cell both twists and bends, taking on a
spiral shape. We tested this mechanism using a mathematical model of expanding fiber-wound
structures and via experiments that measure the shape changes of elongating physical models.
Comparison of the model with *in vivo* experiments on stationary phase *Caulobacter crescentus*
filaments provide the first evidence that mechanical stretching of cytoskeletal fibers influences
cell morphology. Any hydraulic cylinder can spiral by this mechanism if it is reinforced by
stretch-resistant fibers wrapped helically in the same direction, or shortened by contractile
elements. This might be useful in the design of man-made actuators.

1. Introduction

Most bacteria are cylindrical or nearly spherical. However, some bacteria have spiral shapes or grow into spiral filaments if the cells remain connected after dividing. The bacterial cell wall is a polymer mesh of peptidoglycan enclosing the inner membrane bilayer. It provides the cell with the structural reinforcement necessary to resist the cytoplasmic turgor pressure (Arnoldi *et al* 2000). However, the peptidoglycan layer alone does not determine the cylindrical or spiral shape of cells. For example, spirochetes have a spiral shape because of the helically shaped flagella between their inner and outer membranes (Charon and Goldstein 2002, Goldstein *et al* 1994, Ruby *et al* 1997). In this paper, we focus on the mechanism responsible for the spiral shape of other types of bacteria, including single-celled species such as *Caulobacter crescentus* (Fischer *et al* 2002, Wortinger *et al* 1998) and *Vibiro cholerae* (Buddelmeijer *et al* 2002), and species that form long, coiled

filaments of cells, such as *Bacillus subtilis* (Mendelson 1976, Mendelson *et al* 1995).

Rod-shaped bacteria grow by extending along their cylindrical axis of symmetry and then dividing and separating in the middle (Koch 2000, Mendelson 1982). However, certain strains, or mutants, of some species form chains of cells that do not separate upon replication. These multicellular filaments, under particular growth conditions, take on a spiral form and wrap around themselves to produce super-coiled structures reminiscent of tangled telephone cords; examples are *Bacillis subtilis* (Mendelson 1976, Mendelson *et al* 1995), *Bacillus stearothermophilus* (Anagnostopoulus and Sidhu 1979), *Mastigocladus laminosus* (Hernandez-Muniz and Stevens 1988) and *Thermus* sp. (Janssen *et al* 1991) (figure 1). Other bacteria, such as *Caulobacter crescentus* (Fischer *et al* 2002, Wortinger *et al* 1998) and *Vibrio cholera* (Buddelmeijer *et al* 2002), the major causative agent of cholera epidemics (Meno *et al* 1998), form single-celled spiral filaments when starved or stressed. Of these examples, the
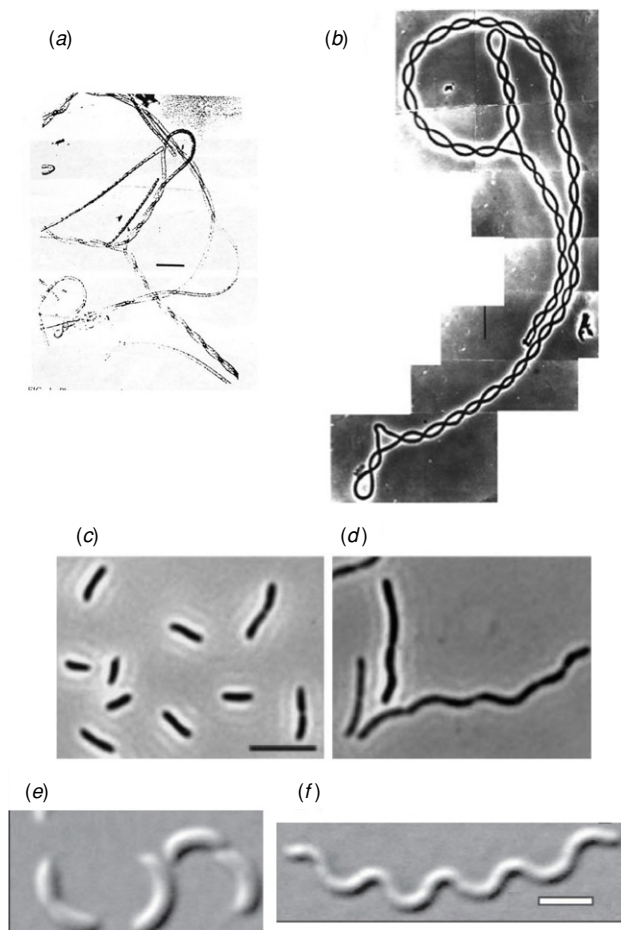
Figure 1. Spiral shapes of bacteria. (*a*) Supercoiled structure of cyanobacterium *M. laminosus* (Hernandez-Muniz and Stevens 1988) (reprinted with permission from Stanley E Stevens). (*b*) Supercoiled structure of *B. subtilis* (Mendelson 1976) (reprinted with permission from National Academy of Sciences). (*c*) *V. cholerae* cells expressing YgbQ and (*d*) with depleted YgbQ (Buddelmeijer *et al* 2002) (reprinted with permission from National Academy of Sciences). (*e*) Exponentially growing and (*f*) stationary phase *C. crescentus* (Ausmees *et al* 2003) (reprinted with permission from Elsevier). Scale bars: 20 μm (*a*), 10 μm (*b*), 10 μm (*c, d*) and 2 μm (*e, f*).

supercoiled filaments of *B. subtilis* have been studied most extensively (Jones *et al* 2001, Mendelson 1976, Mendelson *et al* 1995, Wolgemuth *et al* 2004).

Recent evidence suggests that the actin-like protein fibers, MreB and Mbl, form helices beneath the cell membrane of rod- and spiral-shaped bacterial cells, and appear to play a crucial role in determining and maintaining cell shape (Carballido-Lopez and Errington 2003, Figge *et al* 2004, Jones *et al* 2001, Kurner *et al* 2005). The tensile stresses (forces per cross-sectional area bearing those forces) around the periphery of a cylindrical body with an internal turgor pressure are twice as big in the circumferential direction as in the longitudinal direction (Koehl *et al* 2000, Wainwright 1988). Thus, pressurized cylinders tend to expand radially and become more spherical unless they are reinforced to resist radial expansion. MreB appears to play this role in cylindrical bacteria either by acting as a mechanical strut that provides

direct structural reinforcement or by providing a scaffold that localizes enzymes responsible for cell wall synthesis: when MreB is depleted, the rod-shaped cells of *B. subtilis* (Jones *et al* 2001), *Escherichia coli* (Doi *et al* 1988, Wachi *et al* 1987) and *Caulobacter crescentus* (Figge *et al* 2004) round up. On the other hand, Mbl fibers have been implicated in determining the length and straightness of bacterial cells (Jones *et al* 2001). Cells with a mutated *mbl* gene have an abnormal morphology that is bent and twisted at irregular angles (Jones *et al* 2001). In *B. subtilis*, two Mbl fibers, each at an angle of $\sim$52° relative to the long axis of the cell, wrap helically around the cell in the *same* direction, but 180° out of phase with each other (Jones *et al* 2001). A model by Wolgemuth *et al* (2004) showed that a helical structure with a pitch similar to that of Mbl fibers surrounding a growing bacterial cell can produce the same phenomenon observed in supercoiled multicellular filaments of *B. subtilis*. While *B. subtilis* is wrapped with two helical Mbl fibers, *C. crescentus* is wrapped by a single fiber of an intermediate filament-like protein, which has been implicated in shape determination (Ausmees *et al* 2003).

In this paper, we propose a novel mechanism by which bacteria can take on spiral form when there is a difference between the elongation of the cell and of the cytoskeletal fibers wrapped around it helically. To determine whether this mechanism can produce spiraling, we develop a mathematical model that describes the coupling between elongation of the cell and the extension of the bacterial cytoskeleton, and use the model to predict the shape changes that would occur when a cell or chain of cells lengthens. We test the mathematical model by comparing its predictions to the deformations measured experimentally for physical models of fiber-wrapped elongating cylinders. We use the mathematical and physical models to investigate two separate cases: (1) one cytoskeletal fiber is helically wrapped along the length of the cell and (2) two fibers are wrapped helically in the same direction, but perfectly out of phase with one another. Finally, experiments on stationary phase *C. crescentus* filaments show quantitative agreement with the model and provide the first evidence that mechanical stretching of the bacterial cytoskeleton influences cell morphology.

2. Mechanism of becoming spiral in shape

We propose a mechanism by which a helical fiber—or pair of fibers with the same handedness—wrapped around the periphery of a cylindrical cell, can induce a spiral shape. The essential aspect of our model is that the fiber(s) either extend in length less than the rest of the cell during growth or that the fiber(s) actively shorten or elongate more than the rest of the cell. Thus, our proposed mechanism is applicable if the fiber itself is inextensible, if the fiber actively changes in length, as suggested by Kurner *et al* (2005), or if the fiber directs the orientation of stretch-resistant peptidoglycan molecules in the cell wall (Mbl has been implicated in directing peptidoglycan synthesis (Daniel and Errington 2003)).

Consider a cylindrical bacterial cell (or multicellular filament) with a single polymer fiber attached rigidly to
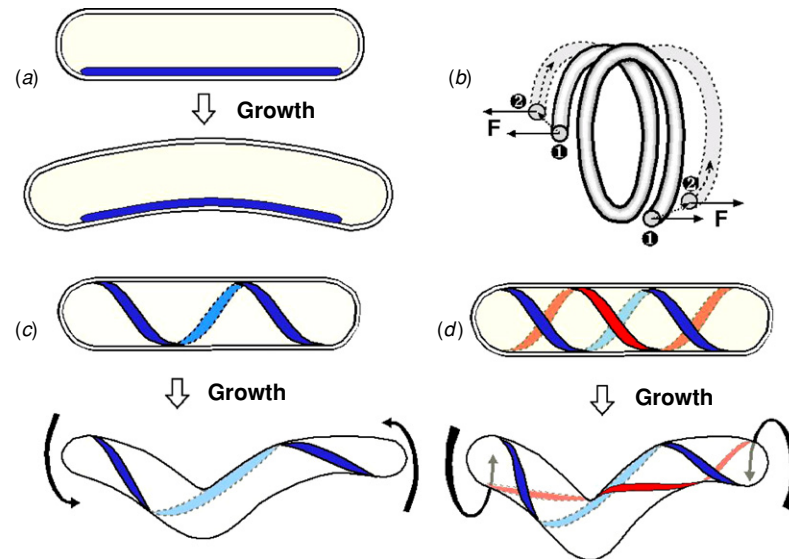
Figure 2. Schematic diagrams of the model. (*a*) A cylindrical bacterium with a polymer fiber adhered to the wall parallel to the long axis. Growth lengthens the bacterium, but the fiber length stays fixed, causing the centerline of the bacterium to bend. (*b*) Stretching a spring produces rotation of the ends in opposite directions. (*c*) A cylindrical bacterium with a helically wrapped polymer fiber adhered to the wall. Growth of the bacterium causes the cell body to twist (black arrows), producing shear stresses in the wall that deforms the cylinder into a spiral shape. (*d*) A cylindrical bacterium with two fibers helically wrapped in the same direction, but 180° out of phase with each other. Growth causes the bacterium to elongate and twist into a spiral shape more pronounced than in the single-fibered case.

the inside of the cell wall parallel to the cell's long axis (figure 2(*a*)). If the cell grows in length but the fiber either remains fixed in length or grows more slowly than the bacterium, the cell will bend into the form of a curved rod, much as changes in temperature bend a bimetallic strip. The same thing occurs if the fiber contracts (i.e., shortens relative to the cell), but the cell bends in the opposite direction if the fiber elongates more than the cell. Now consider a cell around which the polymer fiber is helically wrapped. If you stretch a helical spring, it elongates along its axis and the ends twist in opposite directions (figure 2(*b*)). In a similar manner, elongation of a cell that is wrapped with a helical fiber that does not extend as much as the cell does will cause the cell to twist about its centerline. This will induce shear stresses in the wall of the cell (figure 2(*c*)). Since the cell is elongating faster than the fiber, it also bends with the fiber on the concave side of the bend (as shown in figure 2(*a*)). This combination of twisting and bending curves the cell around into a spiral shape (figure 2(*c*)). If there are two fibers wrapped around the cell in the *same* direction, but perfectly out of phase with one another, then the torsional stresses induced in the wall are greater for a given increase in cell length, and the cell twists more (figure 2(*d*)).

For small to moderate deformations, bacterial cells respond elastically. Experiments using an optical trap measured the bending modulus of filaments of *B. subtilis* and found it to be 1.6×10^{-12} ergs cm (Mendelson *et al* 2000). From this experiment, Young's modulus of the cell wall was estimated to be 5.0 MPa (Mendelson *et al* 2000). Therefore, we model the cell as an elastic object with an inextensible, helically wrapped fiber attached to the wall. As the bending modulus of actin is on the order of 10^{-17} ergs cm (Isambert *et al* 1995, Kas *et al* 1993), we neglect the bending elasticity of

the Mbl fibers relative to the bending elasticity of the bacterial filament.

3. Materials and methods

3.1. Physical models

The design of our physical models was also based on the morphology of *B. subtilis*. Each model was constructed as an inflatable polyurethane cylinder with a resting length-to-diameter ratio equivalent to that of 2.5 cells in a filament. Since filaments of *B. subtilis* cells do not show radial expansion as they grow (Jones *et al* 2001), we embedded circumferentially oriented inextensible threads in the walls of the models to mimic the effect of MreB fibers resisting the diameter increase that would otherwise occur during inflation. In one model, we also embedded two inextensible fibers (ribbons of width = 6.25×10^{-2} of model diameter) in the wall, wrapped helically in the same direction around the model at an angle of 52° to the model's long axis, and out of phase with each other by 180° (*B. subtilis* filaments are composed of individual cells connected together end-to-end but separated by septa. Our model assumes that after septum formation, the Mbl fibers remain in their pre-cell-division alignment and that tensile stress is transmitted between neighboring cells). Another model was wrapped with only one such ribbon at an angle of 52° to the model's long axis.

3.2. Fabrication of physical models

Inflatable polyurethane models of elongating bacteria reinforced with relatively inextensible helically wrapped fibers were constructed using the techniques described by Koehl
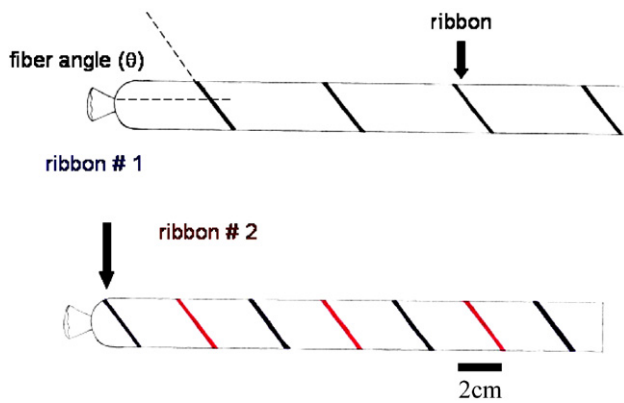
Figure 3. Diagrams of the one-fiber and two-fiber physical models.

et al (2000). A metal rod (diameter = 2.54 cm) served as a mold ('mandrel') for the models. The mandrel surface was lubricated with PAM® (American Home Foods) and then coated with a layer of polyurethane (BJB Enterprises, Shore A polyurethane, type LS-30) that was allowed to polymerize while the mandrel was rotated about its long axis by a motor to maintain an even distribution of the solution as it cured for at least 30 min. A second coat was applied and polymerized on the rotating mandrel in the same way. We then fitted a small hemispherical cap of silk fabric to the rounded end of the model to prevent rupture, and applied a third layer of polyurethane to the model, as described above.

We then embedded relatively inextensible polyester thread (Mölnlycke #9313) in the walls of the models to resist the diameter increase that would otherwise occur during inflation. We wound the thread around the polymerized polyurethane on the mandrel, starting at the proximal end of the model and using ten wraps of the thread per centimeter length of the model. A second thread was then wound around the model with the same spacing and angle, but in the opposite direction, starting at the distal end. This crossed-helical array of threads that were oriented at angles of $+89.3°$ and $-89.3°$ with respect to the long axis of the cylinder (i.e., they were nearly circumferential in orientation) was designed to prevent radial expansion of the model when it was inflated without imposing any twist on it. The model was then coated with another layer of polyurethane, which impregnated the threads when it was applied, and after this layer of polyurethane polymerized on the rotating model, another layer of polyurethane was applied.

We then wrapped the 'two-fiber model' with two relatively inextensible polyester satin ribbons (width = 1.6 mm; C M Offray and Sons), wound helically around the model in the same direction at an angle of $52°$ to the model's long axis and out of phase with each other by $180°$, to mimic the orientation of Mbl fibers in *B. subtilis* (Jones *et al* 2001) (figure 3). Another model, the 'one-fiber model', was wrapped with only one such ribbon at an angle of $52°$ to the model's long axis. The model was then coated with another layer of polyurethane, which impregnated the ribbon when it was applied, and after this layer polymerized, a final coat of polyurethane was applied, and the model was left to cure for 5 days before being removed from the mandrel.

Rows of dots (figures 4(*b*) and (*c*)) were painted on the surface of each model using white correction fluid (Wite-out©, MMM BIC USA, Inc.).

3.3. Inflation of models, measurement of internal pressure and video recording

We elongated each model by inflating it, using the apparatus shown in figure 4(*a*). To avoid effects of gravity and friction on the behavior of the models, we inflated the models with air and then floated them on the surface of a water bath. Each model was clamped to a flexible pipe in series with a pressure gage (Omega PGS-35L-60; full scale $= 414$ kN m^{-2}), a two-way-valve, and a manual air pump (Crank Brothers, Dual Piston Power Pump). After inflating the models to each target pressure (0, 14, 27, 41, 55, 69 and 82 kN m^{-2}, each ± 2 kN m^{-2}), we closed the valve to maintain constant pressure while we videotaped the model. Each model was inflated to each of these pressures during each of five separate replicate experiments. We did not inflate the physical models beyond 82 kN m^{-2} to avoid rupturing them. All measurements were made at room temperature (24 °C).

Models were videotaped in a darkened room using a Sony Handycam Vision color camcorder, DCR-TRV9 affixed above the tank with the lens parallel to the surface of the water in the tank. The floor of the tank was coated with black felt to maximize contrast with the model, which was illuminated through the sides of the tank by two fiber optic lamps (Cole-Parmer Model 9741–50). A wooden ruler floating on the water provided a size scale in the video images.

3.4. Image analysis and measurement of model deformations

Video recordings were converted to Quicktime movies using *iMovie* software. We advanced through the video recordings frame-by-frame using *NIH Image 1.62* software to select the clearest image of the model at each pressure for each of the five replicates of each experiment. These images were used to determine the following measures of model deformation.

3.4.1. Midline length ratio. Midline length ratio is a non-dimensionalized measure of the elongation of the model (figure 4(*b*)). Using *NIH Image 1.62*, we adjusted the black and white contrast of each image until the physical model was white and the background was black, then determined the *x*, *y* coordinates for the points along the top and bottom edges of the model, and used these values to calculate the *x*, *y* coordinates of points along the midline of the model. The distances between these points along the midline were calculated, and their sum was used as midline length. For each of the five replicate experiments conducted on a model, the midline length of the inflated model at a given pressure was divided by its midline length at zero pressure during the same experiment to yield the midline length ratio.

3.4.2. Fiber angle, θ. Fiber angle is the angle of the ribbon(s) with respect to the long axis of model (figure 3). On printouts of the images of the models, we identified points where the
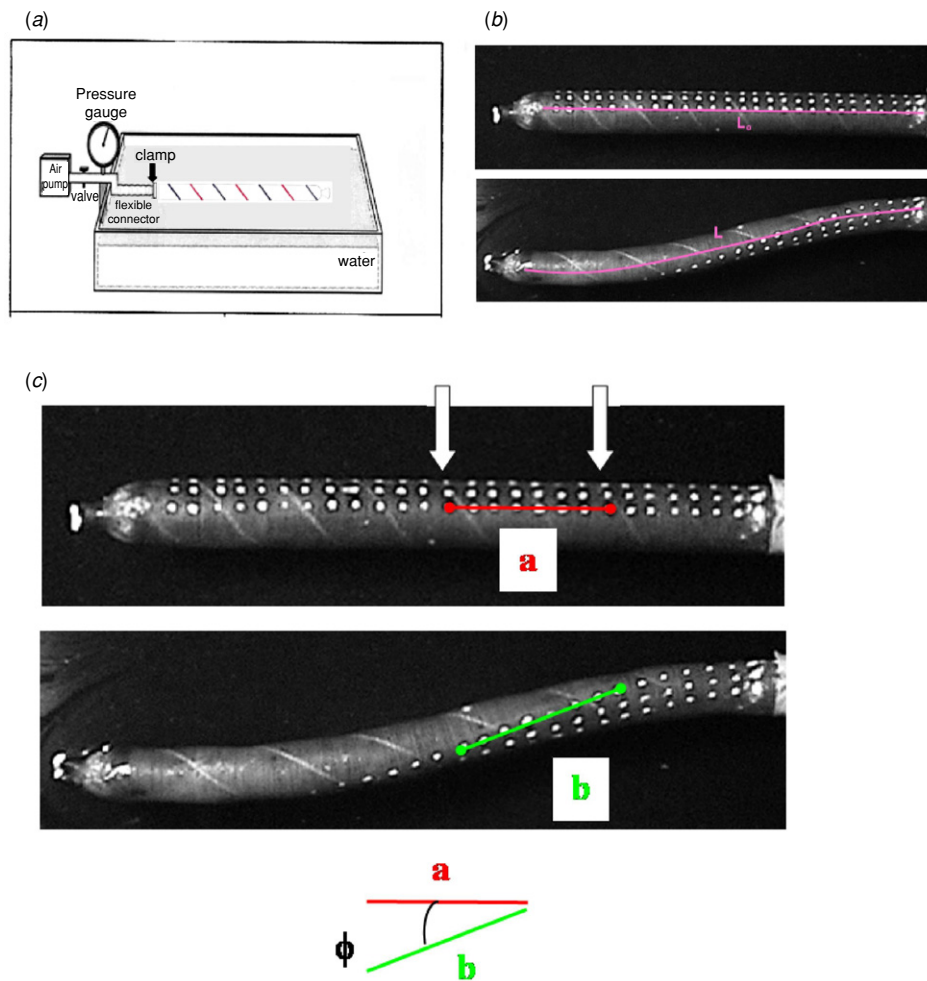
Figure 4. (*a*) Diagram of the apparatus for inflating the physical models. (*b*) Midline length ratio $= L/L_o$. Top: before inflation, bottom: model after inflation. (*c*) Torsion angle, ϕ, and extension ratio. Top: model before inflation, middle: model after inflation, bottom: torsion angle, $\phi =$ the angle between line segments 'a' and 'b'. Extension ratio (stretch of material in wall of model $= b/a$).

ribbons intersected with the midline of the model. We used a protractor to measure the angle (to the nearest degree) between a line drawn with a ruler to be parallel with the local midline and a line drawn to be parallel to the ribbon at each of those points of intersection. The mean of all θ measured for a given pressure in each experiment was used as the θ for that pressure for that replicate.

3.4.3. Extension ratio. Extension ratio is a measure of the longitudinal stretching of the material in the wall of an inflated model (figure 4(*b*)). Because the model twists when it is inflated, a row of dots (marking points on the wall of a model) that was parallel to the long axis of the model when the model was unpressurized were displaced to describe a helix around the model when it was pressurized. We identified seven neighboring dots within a longitudinal row of dots that were near the midline of the model when it was inflated, so that the distances between the dots would not be distorted in the image by the curvature of the model. We divided the distance measured (using *NIH Image 1.62*) between dot #1 and dot #7 (figure 4(*c*)) on the model when inflated to a given pressure,

by the distance between those same dots at zero pressure to calculate extension ratio.

3.4.4. Torsion angle, ϕ. Torison angle, ϕ, is a measure of the amount a model twists when inflated (figure 3). We selected and copied the line segment ('b' in figure 4(*c*)) between the dots (#1 and #7) that were used to measure extension ratio of an inflated model at a particular pressure. We pasted that line segment 'b' onto the image of that same model at zero pressure during the same experiment. We measured the angle, ϕ, between line segment 'b' and the line segment 'a' (figure 4(*c*)) between those same dots in the image of the model at zero pressure.

3.5. Bacterial strains, growth and measurements

C. crescentus strain CJW815 was obtained from C Jacobs-Wagner (Ausmees *et al* 2003) and was grown in peptone–yeast extract (PYE) complex media at 30 °C (Ely 1991). Cell cultures were grown for at least two weeks and up to a month to produce stationary state spiral cells. A Zeiss
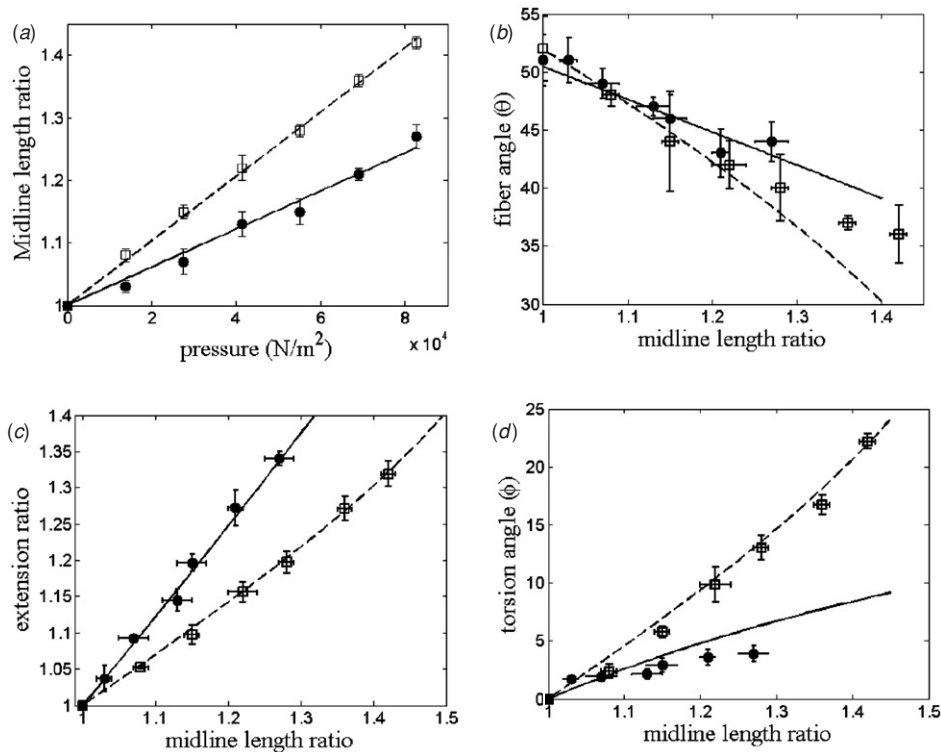
Figure 5. Values calculated for the mathematical models of one-fibered (solid line) and two-fibered (dashed line) cylinders, and measured for one-fibered (black circles) and two-fibered (open squares) physical models. Error bars represent 1 standard deviation ($n = 5$ replicate experiments). (*a*) Midline length ratio of the physical models at different internal pressures, (*b*) fiber angle, θ, between the reinforcing fibers and the local long axis of the model, plotted as a function of midline extension. The mathematical model predicts more pronounced reductions in θ per change in midline length for the two-fibered model, but these differences were not measurable over the range of extensions possible with our physical models. (*c*) Extension ratio (distance between dots painted on the surface of the model divided by the distance between them at zero pressure), a measure of the stretch of the model wall, plotted as a function of midline extension ratio. (*d*) Torsion angle, ϕ (angle between a row of dots on the surface of the model and the line connecting those dots at zero pressure), a measure of the degree of twisting of the model, plotted as a function of midline length ratio.

LSM 510 confocal microscope mounted on an Axiovert 100M with automated xyz control fitted with an Plan-Apochromat objective ($63\times$/1.4 NA Oil objective) and a Perkin-Elmer UltraView spinning disc connected to a Nikon Eclipse TE2000-S microscope with a Plan Apochromat objective ($60\times$/1.4 NA Oil objective) were used to image the cells. Brightfield images were used to measure the average pitch and helix diameter of stationary phase cells using ImageJ software package (developed at the United States National Institutes of Health by Wayne Rasband and available on the internet at http://rsb.info.nih.gov/ij) (see figure 6). The pitch and the diameter were measured at numerous locations along the cell length and averaged. The total cell length was measured using ImageJ by tracing the contour of the cell in an xy image slice.

4. Results and discussion

Solving the equations of our mathematical model for the shape of the cylinder at different lengths, while keeping the fiber length fixed, shows that the cylinder deforms into a spiral shape similar to that observed in the bacteria shown in figure 1 (for a detailed description of the mathematical model, see the

appendices). Similarly, each physical model twisted and bent into a segment of a spiral as it elongated (figures 4(*b*) and (*c*)).

To compare the behavior of our mathematical and physical models, we assessed several aspects of the deformation of the cylinders at a range of extensions. First, we measured the dimensionless extension of the cylinder, defined as the midline length ratio, which is the extended length of the contour midline of the cylinder divided by its initial, uninflated midline length at zero pressure (figure 5(*a*)). For both the one- and two-fiber models, the midline length ratio increased linearly with applied pressure. Therefore, the physical models respond like a linearly elastic filament with constant Young's modulus. We calculated the effective Young's modulus for both physical models and found values of 2.2 kPa for the one-fiber model and 1.5 kPa for the two-fiber model.

As the filament extends, the fiber angle, θ (defined as the angle between the inextensible fiber(s) and the long axis of the cylinder), decreases due to untwisting of the fiber(s) (figure 5(*b*)). For small extensions, the changes in fiber angle due to extension were roughly comparable between the one- and two-fiber models. These changes also agree with the mathematical model.

The extension ratio (a measure of the tensile strain, or stretching, of the wall of the cylinder) increases as the filament

extends (figure 5(*c*)). The one-fiber model shows a greater increase in extension ratio with extension of the filament than the two-fiber model. In contrast, we measured the torsion angle, ϕ (a measure of the amount the cylinder twisted), which increases more for the two-fiber model than the one-fiber model (figure 5(*d*)). This result is due to the fact that for the two-fiber model, the tension in the fibers opposes one another for bending, and, therefore, the filament must twist more. There is good agreement between the predictions of the mathematical model and the measurements on the physical models (figure 5).

Our models permit us to compare the behavior of inflating cylinders reinforced with one fiber versus those reinforced with two fibers wrapped around the cylinder in the same direction. Both models show a linear relationship between internal pressure and midline length, but the two-fiber model elongates more per pressure increase than does the one-fiber model (figure 5(*a*)); however, for a given increase in midline length, the material in the wall of the two-fiber cylinder stretches less than in the one-fiber cylinder (figure 5(*c*)), as the one-fiber model both twists and bends, whereas the two-fiber cylinder deforms mostly by twisting (figure 5(*d*)).

The behavior of our models is consistent with several qualitative observations on bacteria. (1) Our models show that the angle, θ, of the fiber relative to the long axis of the cell decreases as the cell elongates (i.e., the pitch of the fiber becomes greater) (figure 5(*b*)). Similarly, the pitch of Mbl fibers in rapidly elongating *B. subtilis* increases (Carballido-Lopez and Errington 2003), and measured changes in the θ of the Mbl fibers matches our model predictions (Mukherjee *et al* 2005). (2) The mechanism we propose for producing a spiral shape predicts shear stresses in the walls of the twisting, elongating cylinder (figure 5(*d*)). A mechanical model shows that such shear stresses in the wall of a twisting cell can drive the supercoiling motions observed in multicellular spiral filaments of a number of bacterial species (Wolgemuth *et al* 2004) (figures 5(*a*) and (*b*)). (3) Our model predicts that as the cylinder becomes longer, the spiral shape becomes tighter (i.e., the cylinder becomes more curved, so that the radius of the spiral relative to its pitch becomes smaller).

The results of our mathematical model and physical model experiments suggest that bacterial cells in which one helically wrapped cytoskeletal fiber is attached to the cell wall should become more helical as the cell filament elongates. Therefore, as the cell lengthens, both the pitch and the radius of curvature should decrease. *C. crescentus* cells posses two such cytoskeletal filaments, MreB and the intermediate filament-like protein, CreS. During stationary phase, some wild-type cells form long spiral filaments. Mutant cells lacking CreS, however, form long cylindrical filaments. To test our model *in vivo*, we examined filamentous stationary phase *C. crescentus* cells from strain CJW815 (Ausmees *et al* 2003). We measured the average helix diameter, d, and pitch, P, of the cell body as a function of filament length (see figure 6(*a*)). As predicted by the model, both the diameter and pitch decreased as the cell length increased (figures 6(*b*) and (*c*)). During the extension of the cell filament, it is necessary that the CreS fiber also extends. Based on our results, extension of the CreS fiber
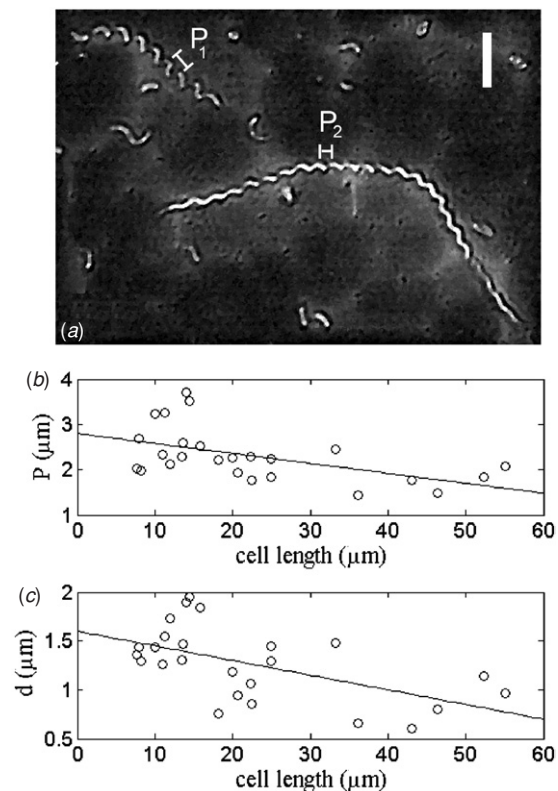

Figure 6. (*a*) Brightfield image of *C. crescenuts* strain CJW815. Two spiral-form stationary phase cells are shown. The pitch of each of these cells, P_1 and P_2, is measured by the distance between neighboring peaks. It is clear that the pitch of the longer filament is shorter than that of the shorter filament. In addition, the shorter filament also has a larger helix diameter than the longer filament. Scale bar: 5 μm. (*b*) Helix pitch versus filament length and (*c*) helix diameter versus filament length for a number of spiral form cells. The black lines are linear fits to the data.

must not be equivalent to the lengthening of the cell filament. As the amount of extension of the CreS fiber is unknown, direct quantitative comparison between the model and the results of the *C. crescentus* experiment was not possible. It is also likely that the elasticity of the CreS fiber will affect the results.

It has been previously suggested that crescentin directly confers spiral form to *C. crescentus* (Ausmees *et al* 2003), i.e., because CreS forms a helical fiber that binds to the cell wall, the cell body is also helical with a pitch and helix diameter that are due to the helicity of crescentin. If this hypothesis is correct, then as the cell filament lengthens, the helix diameter and pitch should not change. Our results show that lengthening of the cell changes the pitch and helix diameter. This result is in agreement with the model presented here that growth of the cell wall that is not equal to the extension of the cytoskeleton twists the cell wall, thereby producing spiral form. The mathematical model that is developed provides a framework with which to begin to explore the mechanisms by which the prokaryotic cytoskeleton produces and maintains cellular morphology. The experiments using the physical models show proof-of-principle the general nature of this model, which provides further evidence that this mechanism may be at play in many non-coccoid bacteria, and, indeed, recent experiments on the

supercoiling of *B. subtilis* are in direct agreement with the results presented here (Mukherjee *et al* 2005).

5. Conclusion and outlook

There are many cases of spiraling and supercoiling in prokaryotes. The mechanical mechanism proposed here for altering shape between spiral and non-spiral forms could be operating in many types of cells that are helically wound with stretch-resistant or contractile fibers. For example, the mechanism we propose can explain why curved-rod bacteria such as *C. crescentus* (Fischer *et al* 2002, Wortinger *et al* 1998) and *V. cholerae* (Buddelmeijer *et al* 2002) become spirals as they lengthen when starved, and why multicellular filaments of many species of bacteria wrap around themselves to form supercoiled structures (Anagnostopoulus and Sidhu 1979, Hernandez-Muniz and Stevens 1988, Janssen *et al* 1991, Mendelson 1976, Mendelson *et al* 1995).

Many biological structures other than bacteria are pressurized cylinders whose walls are wrapped with relatively inextensible fibers (Koehl *et al* 2000, Wainwright 1988), e.g., plant cells, sea anemones, frog notochords, squid tentacles, worms, mammalian tongues), as well as some man-made hydraulic devices (e.g., McKibbon 'muscles'). However, in contrast to the bacteria we have modeled, most of those hydraulic structures are reinforced with a crossed-helical array of fibers (i.e., some fibers wrap around the cylinder in one direction, while others wrap around the cylinder in the *opposite* direction). These structures do not twist or spiral when they extend or shorten because the clockwise and counter-clockwise torques balance (Koehl *et al* 2000, Wainwright 1988). Nevertheless, the principles underlying the models presented here should apply to any hydraulic cylinder that is either reinforced by stretch-resistant fibers all wrapped helically in the same direction around the cylinder or is shortened by contractile elements in such a helical arrangement. It would be interesting to see if such morphologies are found in other spiraling biological structures, such as the tentacles of worms or medusae that coil when retracted, and to explore whether this mechanism of spiraling can be useful in the design of man-made actuators.

Finally, we speculate that the mechanism we have described could be responsible for the spiraling of other cells that have been shown to have MreB homologues, such as the corkscrew shape of Spiroplasma (Trachtenberg 2004), or the transformations between coccoid and spiral shapes at different stages of growth and infection shown by *Helicobacter pylori* (Andersen *et al* 1997, Worku *et al* 1999), the causative agent of gastritis and peptic ulcer disease.
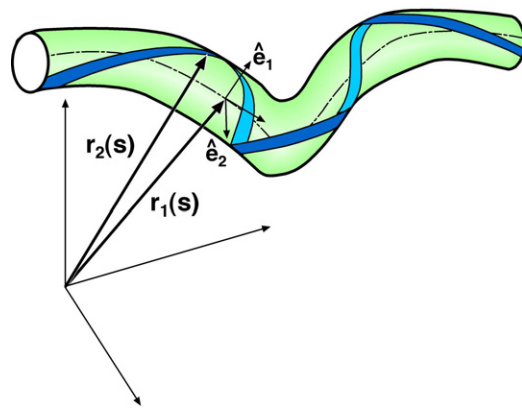
Acknowledgments

Figure 7. Diagrammatic representation of the notation. $\mathbf{r}_1$ is the vector that points to the centerline of the model and $\mathbf{r}_2$ is the vector that points to the helically wrapped ribbon. s is the arclength of the model, describing the distance along the centerline of the model.

Appendices

The configurations shown in figures 2(*b*) and (*c*) can be analyzed mathematically by modeling the cell, or a multicellular filament, as an elastic cylinder that is much longer than it is wide. The helical fibers are inextensible elements adhered to the cell wall, thereby preventing extension of the wall along the fibers. The fibers, which act as tensile elements, are oriented at an angle of 52° to the long axis of the cylinder, and in the two-fiber case, the fibers are 180° out of phase with each other, similar to the arrangement of Mbl fibers in *B. subtilis*.

Appendix A. The one-fiber model

Consider a cylindrically shaped bacterial cell or a chain of connected cells (furthermore called 'the filament') with 1 or 2 inextensible fibers helically wrapped around and embedded in the wall of the filament. We begin by mathematically describing the single-fiber model. The position of the centerline of the filament is defined by the vector $\mathbf{r}_1$ and the position of the fiber is $\mathbf{r}_2$ (see figure 7).

As the fiber is located at the radius of the filament, there is a relationship between $\mathbf{r}_1$ and $\mathbf{r}_2$

$$\mathbf{r}_2 = \mathbf{r}_1 + a\cos\left(\frac{2\pi s_0}{\lambda}\right)\hat{\mathbf{e}}_1 + a\sin\left(\frac{2\pi s_0}{\lambda}\right)\hat{\mathbf{e}}_2 \qquad (A.1)$$

where a is the radius of the filament, λ is the pitch of the fiber on the uninflated filament, s_0 is the arc length of the filament at 0 pressure and $\hat{\mathbf{e}}_1$ and $\hat{\mathbf{e}}_2$ are the unit vectors perpendicular to the long axis of the filament. The fiber angle, θ, is the angle between the axis of the midline of the cylinder and the angle of the fiber. The cosine of θ is the angle between the tangents of $\mathbf{r}_1$ and $\mathbf{r}_2$

$$\cos\theta = \frac{\partial\mathbf{r}_1}{\partial s}\cdot\frac{\partial\mathbf{r}_2}{\partial s_2} \qquad (A.2)$$

where s is the arc length along the extended filament and s_2 is the arc length along the fiber.

The filament is considered to be an elastic strand that is straight at equilibrium. Therefore, the elastic deformation energy (the strain energy stored in the deformed material of the cell wall) can be defined as

$$E_{\text{el}} = \int \left(\frac{A}{2} (\Omega_1^2 + \Omega_2^2) + \frac{C}{2} \Omega_3^2 \right) \mathrm{d}s \qquad (A.3)$$

where Ω_1 and Ω_2 are the curvatures about $\hat{\mathbf{e}}_1$ and $\hat{\mathbf{e}}_2$, respectively, and Ω_3 is the twist density (twist per length). The constants A and C characterize the elastic stiffness of the filament in bending and twist, respectively. The fiber is assumed to be inextensible. Therefore,

$$\varepsilon^2 \left(\frac{\partial \mathbf{r}_2}{\partial s} \cdot \frac{\partial \mathbf{r}_2}{\partial s} \right) = \gamma^2 = \text{constant} = \left(\frac{L_f}{L_0} \right)^2 = 1 + \left(\frac{2\pi a}{\lambda} \right)^2 \qquad (A.4)$$

where ε is the midline length ratio of the filament, $\gamma = L_c/L_0$, is the ratio of the fiber length, L_f, to the length of the filament at zero pressure, L_0. From (A.2) and (A.4), we find

$$\cos\theta = \frac{\varepsilon}{\gamma} \left(1 - a\,\Omega_2 \cos\left(\frac{2\pi s_0}{\lambda} \right) + a\,\Omega_1 \sin\left(\frac{2\pi s_0}{\lambda} \right) \right). \qquad (A.5)$$

We also define a constraint energy (the tensile energy stored in the fiber because it cannot extend) to impose the inextensibility condition for the fiber

$$E_c = \int \Lambda \left(\gamma - \frac{L_f}{L_0} \right) \mathrm{d}s_0 \qquad (A.6)$$

where Λ is a Lagrange multiplier and L_R is the length of the fiber. The total energy for the model system is $E_t = E_{\text{el}} + \underline{E_c}$. The force per unit length, $\mathbf{f}$, that acts along the filament is the functional derivative of the total energy with respect to $\mathbf{r}_1$

$$\mathbf{f} = -\frac{\delta E_t}{\delta \mathbf{r}_1}. \qquad (A.7)$$

The twisting moment, m, about the tangent vector of the centerline of the filament is given by

$$m = -\frac{\delta E_t}{\delta \chi} \qquad (A.8)$$

where $\delta\chi$ is the angle around $\hat{\mathbf{e}}_3$ through which $\hat{\mathbf{e}}_1$ rotates as it moves to $\hat{\mathbf{e}}_1 \to \hat{\mathbf{e}}_1 + \delta\hat{\mathbf{e}}_1$.

If the filament is not moving, the force and moment per length are zero along the entire length, $\mathbf{f} = m = 0$. In the absence of external forces, the total force, $\mathbf{F}$, and total moment, $\mathbf{M}$, at the ends of the filament are zero. For an elastic filament, the force and moment are related by (Landau and Lifshitz 1985)

$$\frac{\partial \mathbf{M}}{\partial s} - \mathbf{F} \times \frac{\partial \mathbf{r}}{\partial s} = 0. \qquad (A.9)$$

Since the force per length is zero everywhere, and $\mathbf{F} = 0$ on the boundary, $\mathbf{F}$ must be zero everywhere along the filament.

Integrating (A.9) with the boundary condition gives $\mathbf{M} = 0$. Therefore, the following conditions apply:

$$\Omega_2 \cos\left(\frac{2\pi s_0}{\lambda} \right) - \Omega_1 \sin\left(\frac{2\pi s_0}{\lambda} \right) = \frac{a\Lambda\varepsilon^2}{\gamma A + a^2\Lambda\varepsilon^2}$$

$$\Omega_2 \sin\left(\frac{2\pi s_0}{\lambda} \right) + \Omega_1 \cos\left(\frac{2\pi s_0}{\lambda} \right) = 0 \qquad (A.10)$$

$$\Omega_3 = -\left(\frac{2\pi a}{\lambda} \right) \frac{a\Lambda\varepsilon}{\gamma C + a^2\Lambda\varepsilon^2}.$$

Using this model, we can calculate the parameters measured on the physical models.

A.1. Calculation of the midline length as a function of pressure

If we assume that the filament is a linearly elastic object, then the expansion of the midline length ratio, ε, should be proportional to the applied pressure

$$\varepsilon = \pi a^2 Y P \qquad (A.11)$$

where Y is Young's modulus (i.e., resistance to stretching) of the cell wall of the filament and P is the internal pressure.

A.2. Calculation of the fiber angle, θ

Inserting (A.10) into (A.5), we find

$$\cos\theta = \frac{\varepsilon}{\gamma} \left(1 - \frac{a^2\Lambda\varepsilon}{\gamma A + a^2\Lambda\varepsilon} \right) \qquad (A.12)$$

(A.4) and (A.10) give three equations in three unknowns from which we can solve for Λ. However, rather than solving for Λ it is easier to make the definition

$$\alpha = \frac{a^2\Lambda\varepsilon}{\gamma A + a^2\Lambda\varepsilon^2}. \qquad (A.13)$$

Assuming that $A = C$ and using (A.4), (A.10) and (A.13), we find that

$$\alpha = \frac{1}{a\varepsilon} \left[1 - \frac{\gamma}{(\varepsilon^2 + \gamma^2 - 1)^{\frac{1}{2}}} \right]. \qquad (A.14)$$

Therefore, α is a function of γ and the midline length ratio. Solving (A.14) for α and using (A.12), the fiber angle, θ, can be calculated as a function of midline length ratios :

$$\theta = \arccos\left(\frac{\varepsilon}{\gamma}(1 - \alpha) \right). \qquad (A.15)$$

Comparing (A.15) to the data gives $\gamma = 1.57$ or an initial fiber angle of $50.4°$.

A.3. Calculation of the torsion angle, ϕ

The torsion angle, ϕ can be calculated as a function of midline length ratio and can be compared with measured torsion angles for the physical models if we assume that the dots that are painted on the physical model are aligned with the $\hat{\mathbf{e}}_1$ direction. Therefore, the vector that points to the dots is

$$\mathbf{r}_d = \mathbf{r}_1 + a\hat{\mathbf{e}}_1. \qquad (A.16)$$

The cosine of the torsion angle is

$$\cos\phi = \frac{\partial \mathbf{r}_d}{\partial s_d} \cdot \frac{\partial \mathbf{r}_1}{\partial s} = \frac{(1 - a\Omega_2)}{\left((1 - a\Omega_2)^2 + a^2\Omega_3^2\right)^{1/2}} \quad \text{(A.17)}$$

where s_d is the arc length along the line that connects the painted dots. The conditions (A.10) imply that

$$a\Omega_2 = \alpha \cos\left(\frac{2\pi s_0}{\lambda}\right). \quad \text{(A.18)}$$

If we look at a fixed position in s_0, then $a\Omega_2 = \alpha \cos\beta$, where β is a constant and

$$\phi = \arccos\left(\frac{(1 - \alpha\cos\beta)}{((1 - \alpha\cos\beta)^2 + (\gamma^2 - 1)\alpha^2)^{\frac{1}{2}}}\right). \quad \text{(A.19)}$$

Comparing (A.19) to the data for ϕ from the one-fiber model gives $\beta = 121°$.

A.4. Calculation of the extension ratio, ER

The extension ratio, ER, is the stretch of the material in the filament wall. It can be measured on the physical model as the distance between adjacent dots painted on the surface of the filament divided by the initial distance between those dots. Therefore, the extension ratio, ER, is

$$\begin{aligned}
\text{ER} &= \varepsilon\left(\frac{\partial \mathbf{r}_d}{\partial s} \cdot \frac{\partial \mathbf{r}_d}{\partial s}\right)^{\frac{1}{2}} \\
&= \varepsilon((1 - \alpha\cos\beta)^2 + (\gamma^2 - 1)\alpha^2). \quad \text{(A.20)}
\end{aligned}$$

The same value of β as was found above ($\beta = 121°$) provides good agreement with the data for ER (see figure 5 in the main text).

Appendix B. The two-fiber model

For the two-fiber model, another fiber is added $180°$ out of phase with respect to the first fiber but with the same handedness. Therefore, the vector that describes the position of this second fiber is

$$\mathbf{r}_3 = \mathbf{r}_1 - a\cos\left(\frac{2\pi s_0}{\lambda}\right)\hat{\mathbf{e}}_1 - a\sin\left(\frac{2\pi s_0}{\lambda}\right)\hat{\mathbf{e}}_2. \quad \text{(B.1)}$$

This fiber is also assumed to be inextensible. Therefore,

$$\varepsilon^2\left(\frac{\partial \mathbf{r}_3}{\partial s} \cdot \frac{\partial \mathbf{r}_3}{\partial s}\right) = \gamma_2^2 = \left(\frac{L_f}{L_0}\right)^2. \quad \text{(B.2)}$$

The only way both (A.4) and (B.2) can hold simultaneously is if

$$\Omega_2\cos\left(\frac{2\pi s_0}{\lambda}\right) - \Omega_1\sin\left(\frac{2\pi s_0}{\lambda}\right) = 0. \quad \text{(B.3)}$$

This implies that

$$\gamma^2 = \gamma_2^2 = \varepsilon^2 + \left(\frac{2\pi a}{\lambda} + a\varepsilon\Omega_3\right)^2. \quad \text{(B.4)}$$

B.1. Calculation of the midline length ratio

As in the one-fiber model, we assume that the filament is linearly elastic with respect to extension of the midline length ratio with applied pressure. Therefore, we use (A.11) to calculate the midline length ratio.

B.2. Calculation of the fiber angle, θ

Using (A.24), we can maintain the same definition of the constraint energy, E_c (A.6), and define the force, $\mathbf{f}$, and moment, m, using (A.7) and (A.8), respectively. Putting (A.23) and (A.24) into (A.5), we find the equation for the fiber angle, θ, versus midline length ratio, ε,

$$\cos\theta = \frac{\varepsilon}{\gamma}. \quad \text{(B.5)}$$

Comparison of this calculated θ to the measurement of θ on the two-fiber physical model gives $\gamma = 1.62$, which is equivalent to an initial fiber angle of $52°$. For the two-fiber model we get the same relation for the twist density, Ω_3, as in the one-fiber model

$$\begin{aligned}
\Omega_3 &= -\left(\frac{2\pi a}{\lambda}\right)\frac{a\Lambda\varepsilon}{\gamma C + a^2\Lambda\varepsilon} \\
&= -(\gamma^2 - 1)^{\frac{1}{2}}\alpha \quad \text{(B.6)}
\end{aligned}$$

where α is as defined in (A.13), with $C = A$.

B.3. Calculation of the torsion angle and extension ratio

The torsion angle, ϕ, and extension ratio, ER, can be calculated using (A.19) and (A.20). For the two-fiber model, we find a value $\beta = 60°$.

Glossary

Mreb/Mbl. Bacterial polymer homologous to actin in eukaryotes.

Stress. Force per cross-sectional area bearing that stress.

Supercoiling. The process whereby a filamentous, interconnected chain of bacteria wraps itself into a structure resembling an overtwisted phone cord.

Young's modulus. The ratio of stress to strain, a measure of the stiffness of a given material.

References

Anagnostopoulos G D and Sidhu H S 1979 Helical growth of *Bacillus stearothermophilus* in low water activity media *Microbios. Lett.* **5** 115–21

Andersen A P, Elliott D A, Lawson M, Barland P, Hatcher V B and Puszkin E G 1997 Growth and morphological transformations of *Helicobacter pylori* in broth media *J. Clin. Microbiol.* **35** 2918–22

Arnoldi M, Fritz M, Bauerlein E, Radmacher M, Sackmann E and Boulbitch A 2000 Bacterial turgor pressure can be measured by atomic force microscopy *Phys. Rev.* E **62** 1034–44

Ausmees N, Kuhn J R and Jacobs-Wagner C 2003 The bacterial cytoskeleton: an intermediate filament-like function in cell shape *Cell* **115** 705–13

Buddelmeijer N, Judson N, Boyd D, Mekalanos J J and Beckwith J 2002 YgbQ, a cell division protein in *Escherichia coli* and *Vibrio cholerae*, localizes in codependent fashion with FtsL to the division site *Proc. Natl Acad. Sci. USA* **99** 6316–21

Carballido-Lopez R and Errington J 2003 The bacterial cytoskeleton: *in vivo* dynamics of the actin-like protein Mbl of *Bacillus subtilis Dev. Cell* **4** 19–28

Charon N W and Goldstein S F 2002 Genetics of motility and chemotaxis of a fascinating group of bacteria: the spirochetes *Annu. Rev. Genet.* **36** 47–73

Daniel R and Errington J 2003 Control of cell morphogenesis in bacteria: two distinct ways to make a rod-shaped cell *Cell* **113** 767–76

Doi M, Wachi M, Ishino F, Tomioka S, Ito M, Sakagami Y, Suzuki A and Matsuhashi M 1988 Determinations of the DNA sequence of the mreB gene and of the gene products of the mre region that function in formation of the rod shape of *Escherichia coli J. Bacteriol.* **170** 4619–24

Ely B 1991 Genetics of *Caulobacter crescentus Methods Enzymol.* **204** 372–84

Figge R N, Divakaruni A V and Gober J W 2004 MreB, the cell shape-determining bacterial actin homologue, co-ordinates cell wall morphogenesis in *Caulobacter crescentus Mol. Microbiol.* **51** 1321–32

Fischer B, Rummel G, Aldridge P and Jenal U 2002 The FtsH protease is involved in development, stress response and heat shock control in *Caulobacter crescentus Mol. Microbiol.* **44** 461–78

Goldstein S F, Charon N W and Kreiling J A 1994 *Borrelia burgdorferi* swims with a planar waveform similar to that of eukaryotic flagella *Proc. Natl Acad. Sci. USA* **91** 3433–7

Hernandez-Muniz W and Stevens S E 1988 Significance of braided trichomes in the cyanobacterium *Mastigocladus laminosus J. Bacteriol.* **170** 1519–22

Isambert H, Venier P, Maggs A, Fattoum A, Kassab R, Pantaloni D and Carlier M-F 1995 Flexibility of actin filaments derived from thermal fluctuations. Effect of bound nucleotide, phalloidin, and muscle regulatory proteins *J. Biol. Chem.* **270** 11437–44

Janssen P H, Parker L E and Morgan H W 1991 Filament formation in *Thermus* species in the presence of D-amino acids or glycine *Antonie van Leeuwenhoek* **59** 147–54

Jones L J, Carballido-Lopez R and Errington J 2001 Control of cell shape in bacteria: helical, actin-like filaments in *Bacillus subtilis Cell* **104** 913–22

Kas J, Strey H, Barmann M and Sackmann E 1993 Direct measurement of the wave-vector-dependent bending stiffness of freely flickering actin filaments *Europhys. Lett.* **21** 865–70

Koch A L 2000 The bacterium's way for safe enlargement and division *Appl. Environ. Microbiol.* **66** 3657–63

Koehl M A R, Quillin K J and Pell C A 2000 Mechanical design of fiber-wound hydraulic skeletons: the stiffening and straightening of embryonic notochords *Am. Zool.* **40** 28–41

Kurner J, Frangakis A S and Baumeister W 2005 Cryo-electron tomography reveals the cytoskeletal structure of *Spiroplasma melliferum Science* **307** 436–8

Landau L D and Lifshitz E M 1985 *Theory of Elasticity* (Oxford: Butterworth-Heinemann)

Mendelson N H 1976 Helical growth of *Bacillus subtilis*: a new model of cell growth *Proc. Natl Acad. Sci. USA* **73** 1740–4

Mendelson N H 1982 Bacterial growth and divison: genes, structures, forces, and clocks *Microbiol. Rev.* **46** 341–75

Mendelson N H, Sarlls J E, Wolgemuth C W and Goldstein R E 2000 Chiral self-propulsion of growing bacterial macrofibers on a solid surface *Phys. Rev. Lett.* **84** 1627–30

Mendelson N H, Thwaites J J, Kessler J O and Li C 1995 Mechanics of bacterial macrofiber initiation *J. Bacteriol.* **177** 7060–9

Meno Y, Waldor M K, Mekalanos J J and Amako K 1998 Morphological and physical characterization of the capsular layer of *Vibrio cholerae* 0139 *Arch. Microbiol.* **170** 339–44

Mukherjee S, Setlow B, Setlow P and Wolgemuth C W 2005 Growing pains and the bacterial cytoskeleton, unpublished

Ruby J D, Li H, Kuramitsu H, Norris S J, Goldstein S F, Buttle K F and Charon N W 1997 Relationship of *Treponema denticola* periplasmic flagella to irregular cell morphology *J. Bacteriol.* **179** 1628–35

Trachtenberg S 2004 Shaping and moving a Spiroplasma *J. Mol. Microbiol. Biotechnol.* **7** 78–87

Wachi M, Doi M, Tamaki S, Park W, Nakajima-Iijima S and Matsuhashi M 1987 Mutant isolation and molecular cloning of mre genes, which determine cell shape, sensitivity to mecillinam, and amount of penicillin-binding proteins in *Escherichia coli J. Bacteriol.* **169** 4935–40

Wainwright S A 1988 *Axis and Circumference* (Cambridge, MA: Harvard University Press)

Wolgemuth C W, Goldstein R E and Powers T R 2004 Dynamic supercoiling bifurcations of growing elastic filaments *Physica* D **190** 266–89

Worku M L, Sidebotham R L, Walker M M, Keshavarz T and Karim Q N 1999 The relationship between *Helicobacter pylori* motility, morphology and phase of growth: implications for gastric colonization and pathology *Microbiology* **145** 2803–11

Wortinger M A, Quardokus E M and Brun Y V 1998 Morphological adaptation and inhibition of cell division during stationary phase in *Caulobacter crescentus Mol. Microbiol.* **29** 963–73